# Supporting Information

## Inducing Piezoelectric Behavior in Copper Iodide Cubane Cluster-Based Metal-Organic Framework via Linker Engineering

Sankalpa N. Panda,[†,‡,#] Prabhanjan Pradhan,[ꟷ,$,#] Satyapriya Nath,[†,‡] Jeebanjyoti Mohapatra,[†,‡] Biplab K. Patra[ꟷ,$,*], and Bishnu P. Biswal[†,‡,§,*]

[†]School of Chemical Sciences, National Institute of Science Education and Research Bhubaneswar, Jatni, Khurda, Odisha, 752050, India

[‡]Homi Bhabha National Institute, Training School Complex, Anushakti Nagar, Mumbai, 400094, India

[§]Centre for Interdisciplinary Sciences, National Institute of Science Education and Research Bhubaneswar, Jatni, Khurda, Odisha, 752050, India

[ꟷ]Materials Chemistry Department, CSIR-Institute of Minerals and Materials Technology, Bhubaneswar, Odisha 751013, India

[$]Academy of Scientific and Innovative Research (AcSIR), Ghaziabad 201002, India

[#]These authors contributed equally to the work.

**Email:** bp.biswal@niser.ac.in; bkpatra@immt.res.in

# Table of Contents

# Section S-1: Materials and instrumentation

**Materials**

All commercially available reagents and solvents were used without further purification. Depending upon availability, commercially available starting materials were bought from Sigma-Aldrich, TCI Chemicals, and BLD Pharma.

**General instrumentation and methods:**

**Powder X-ray diffraction (PXRD)** patterns were collected at room temperature on a Bruker D8 Advance X-ray powder diffractometer with Cu Kα radiation ($\lambda = 1.5418$ Å) as the X-ray source.

**Fourier transform infrared (FT-IR)** spectra were recorded using a Vertex 70 FT-IR spectrometer (Bruker, Germany) equipped with an attenuated total reflectance (ATR) accessory. The spectra were background corrected and reported with a wave number ($cm^{-1}$) scale. The transmittance spectra were collected in the 3500-500 $cm^{-1}$ range with a scan velocity of 7.5 kHz.

**Thermogravimetric analyses (TGA)** were carried out on a TG50 analyzer (Mettler-Toledo) and an SDT Q600 TG-DTA analyzer in the nitrogen at a heating rate of 5 ºC $min^{-1}$ within a temperature range of 25−800 °C.

**Scanning electron microscopy (SEM)** measurements were executed with a Merlin Compact field effect SEM (FESEM) with a GEMINI-I electron column, Zeiss Pvt. Ltd., Germany. The samples were prepared by sonicating in isopropyl alcohol (IPA) for 1 hour and drop-casting on silicon wafers for the powder sample, and crystals directly attached to silicon wafers using carbon tape.

**UV-Visible diffused reflectance spectroscopy (UV-Vis DRS)** spectroscopy was carried out, and the absorption spectra of both crystals were recorded with an Agilent Cary spectrophotometer.

**$N_2$ Sorption analyses** were performed at 77 K on a Quantachrome Instruments Autosorb iQ automatic volumetric instrument. All the samples were outgassed for 12 h at 100 °C under the vacuum before the gas adsorption studies. The surface areas were evaluated using the Brunauer-Emmett-Teller (BET) model applied between $P/P_0$ values of 0.05 and 0.3.

**Piezo force microscopy (PFM)** was employed to investigate the piezoelectric nature of the crystals using the Piezo response force imaging mode of atomic force microscope (Bruker Nano Wizard Sense+ Bio-AFM) in contact mode. For all PFM measurements, a conductive tip (Model- CONTV PT) having a spring constant of 0.2 N/m and resonance frequency of 13 kHz was used. During the measurements, the voltage was applied to the tip, and the ITO glass on which the sample was placed was kept grounded. The PFM images were recorded at a drive frequency of 37.2 kHz. All the recorded PFM images were analyzed using JPK data processing software.

**Switching spectroscopy piezo force microscopy (SS-PFM)** mode was used to measure the nanoscale domain switching of the sample using an atomic force microscope (Bruker Nano Wizard Sense+ Bio-AFM). For all ss-PFM measurements, a conductive tip (Model- CONTV PT) having a spring constant of 0.2 N/m and a resonance frequency of 13 kHz was employed. During the

measurements, the voltage was applied to the tip, and the bottom Ag-coated ITO glass was kept grounded. The PFM images were recorded at a resonance frequency of 37.2 kHz by applying two oscillating voltages. The characteristic PFM phase and amplitude curves of the sample were observed by applying triangular pulses ranging from ±50V up to ±80V. For non-centrosymmetric materials, the amplitude of the cantilever (Amp) is determined by the converse piezoelectric effect and can be expressed as

$$Amp(cantilever) = d_{33} \times V_{applied}$$

We measured the amplitude signal by varying the bias and subsequently calculated the $d_{33}$ values using this equation.

For our system Amplitude= 4.1861nm and Voltage=80V

So $d_{33}$=4.1861nm /80V=0.05232nm/V=52.32pm/V.

**Piezoelectric nanogenerator (PENG)** output voltage responses to various pressure modes were measured using a Keithley 6517B system.

**JSGW UV Cabinet** was utilized to capture images of photoluminescent active crystals under the illumination of 365 nm UV light.

# Section S-2: Synthesis procedures

**Synthesis of Cu$_4$I$_4$(DABCO)$_2$:**

For the synthesis of Cu$_4$I$_4$(DABCO)$_2$ powder, we have followed the previously reported method by Braga *et al*. In this method, 1,4-diazabicyclo [2.2.2]octane (DABCO)(0.134 gm, 1.2 mmol) was dissolved in 15 mL of acetonitrile at 70° and added under stirring to a solution of CuI (0.190 g, 1 mmol) in acetonitrile (15 mL) at 70°C. Upon addition, the solution became turbid, followed by the precipitation of a white powder. It was left stirring in solution at 70°C for about 3 hours to ensure completion of the reaction. The solid material was recovered by centrifugation and washed with water and acetone, respectively. Then, the precipitate was dried under a vacuum to obtain the product Cu$_4$I$_4$(DABCO)$_2$ with c.a. 65% yield.

***FT-IR :( 3500-500 cm$^{-1}$***): 2952 (w), 2878 (w), 1709(w), 1458(w), 1319(w), 1047(m), 998(m), 910(w), 834(m), 794(s), 770(m)

***Elemental analysis***: Calcd. (%) C, 15.6; H, 2.7; N, 5.6; Found (%): C, 14.7; H, 2.15; N, 4.7

**Crystallization of Cu$_4$I$_4$(DABCO)$_2$:**

A three layers crystallization procedure was used to obtain a single crystal of a similar product, where a solution of DABCO in acetone was taken in the top layer, toluene in the middle, and CuI with a saturated aqueous solution of KI was kept as the bottom layer. The crystals appeared in the bottom layer after 5-7 days, which is characterized using single-crystal X-ray diffraction method.

**Crystallization of Cu$_4$I$_4$(Pip)$_2$:**

A three layers crystallization procedure was used to obtain the single crystal, where a solution of piperazine in acetone was taken in the top layer, toluene in the middle, and CuI with a saturated aqueous solution of KI was kept as the bottom layer. The crystals appeared in the bottom layer after 3-5 days (Yield: 41 %), characterized using single-crystal X-ray diffraction method.

***FT-IR :(3500-500 cm$^{-1}$):*** 3230 (w), 2943 (w), 1445 (w), 1339(w), 1244(m), 1096(m), 1047(m), 990(s), 865(s), 625(m)

***Elemental analysis:*** Calcd. (%) C, 12.51; H, 2.3; N, 5.84; Found (%): C, 12.52; H, 1.97; N, 4.26.

**Preparation of the composite film:**

The composite used for the device fabrication was prepared by mixing the Cu$_4$I$_4$(Pip)$_2$ with an adequate amount of the poly(methyl methacrylate) abbreviated as PMMA. 5, 10, 15, and 20 % w/w films were prepared using stoichiometric amount of Cu$_4$I$_4$(Pip)$_2$ powder obtained by grinding the crystals. For composite film fabrication, firstly, the Cu$_4$I$_4$(Pip)$_2$ powder was dispersed in 1 mL of DMF by stirring for 30 minutes at room temperature to get a homogenous dispersion. Subsequently,

a calculated amount of PMMA was added to the solution and stirred until the PMMA dissolves completely. The resultant solution was drop casted on a precleaned glass slide and dried at room temperature for 30 minutes. The slides were dried in a vacuum oven at 80 °C for 4 hours to get uniform free-standing films. The stoichiometric ratio of $Cu_4I_4(Pip)_2$ and PMMA is given below.

| Film | $Cu_4I_4(Pip)_2$ Quantity (mg) | PMMA Quantity (mg) |
|---|---|---|
| 5 wt % | 1.5 | 28.5 |
| 10 wt % | 3 | 27 |
| 15 wt % | 4.5 | 25.5 |
| 20 wt % | 6 | 24 |

**Fabrication of Nanogenerators**:

The obtained composite films are cut into 2 cm × 2 cm. The nanogenerators were prepared with copper wires, which are affixed to the composite films using adhesive copper tape, serving as the electrodes. The entire assembly was then thoroughly laminated to facilitate easy and safe handling.

# Section S-3: Single crystal X-ray diffraction analysis of MOFs

The $Cu_4I_4(Pip)_2$ MOF was crystalized using the three-layer solvent diffusion method at room temperature. White crystals appeared after 3-5 days, which was suitable for single crystal X-ray diffraction (SCXRD) measurement. The SCXRD Data was collected on a Rigaku Oxford XtaLAB SuperNova (microfocus) (Rigaku, v1.171.42.89a, 2023) equipped with a CCD area detector and operated at 250 W power (50 kV, 0.8 mA) to generate Mo Kα radiation ($\lambda$ = 0.71073 Å) and Cu Kα radiation ($\lambda$ = 1.54184 Å) at 100 K-276 K. For the measurement of the crystal reported in this paper, we have used Cu Kα radiation ($\lambda$ = 1.54184 Å) at 113 K and for mounting we have used nylon Cryo loops (Hampton Research) with Paraton-N (Hampton Research). A preliminary set of reflections is needed to determine preliminary unit cell parameters and assess the mosaicity (breadth of spots between frames) of the crystal to select the required frame width for data collection. A short pre-experiment with 1 Å resolution was run, from which an optimal data collection strategy was determined. The range of θ was from 5.7740 to 77.5420°. The full data set was collected with a 2-s exposure time throughout all angles. A series of frames were collected in 0.50 steps. $Cu_4I_4(Pip)_2$ MOF was crystalized in the $P6_222$ hexagonal space group with an asymmetric unit containing one Cu atom, one I atom, and half of the piperazine ligand. After the intensity data were corrected for absorption, the final cell constants were calculated from the XYZ centroids of 11234 strong reflections from the actual data collection after integration. The structure was determined using direct methods employed in SHELXT,[1] Olex2,[2] and refinement was carried out using least-square minimization implemented in SHELXL.[3] All non-hydrogen atoms were refined with anisotropic displacement parameters. All hydrogen atom's positions were fixed geometrically in idealized positions and were refined using a riding model. The final full matrix least squares refinement converged to R1 = 0.0539 (F2, I > 2 sec (I)) and wR2 = 0.1589 (F2, all data). The refinement was carried out in Olex2 (1.3). The crystal packing images were generated using diamond software from Crystal Impact. Table S1 summarizes the selected bond lengths for the structure. Table S4 provides a summary of the crystal data and structure refinement parameters for the structural studies of $Cu_4I_4(Pip)_2$. The supplementary crystallographic data of the structures $Cu_4I_4(Pip)_2$ have been deposited in the CCDC database (CCDC 2394021)".
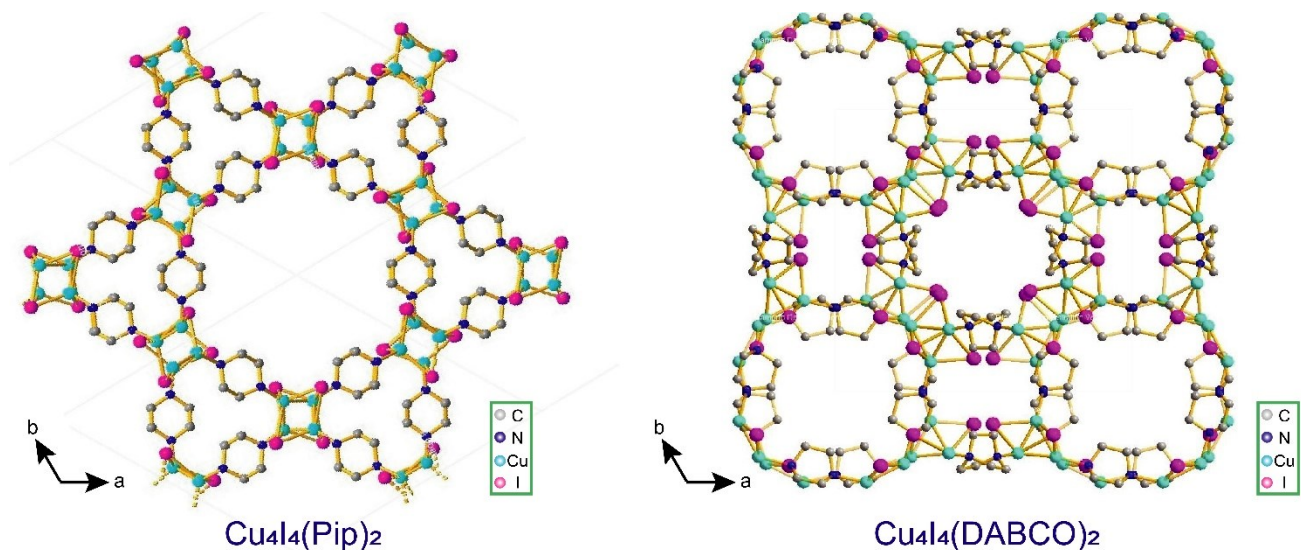
**Figure S1.** Single crystal XRD structure (ball and stick model) of $Cu_4I_4(Pip)_2$ and $Cu_4I_4(DABCO)_2$ along the c-axis, H atoms have been omitted for clarity. *C*, grey; *N*, blue; *Cu*, cyan; *I*, pink.
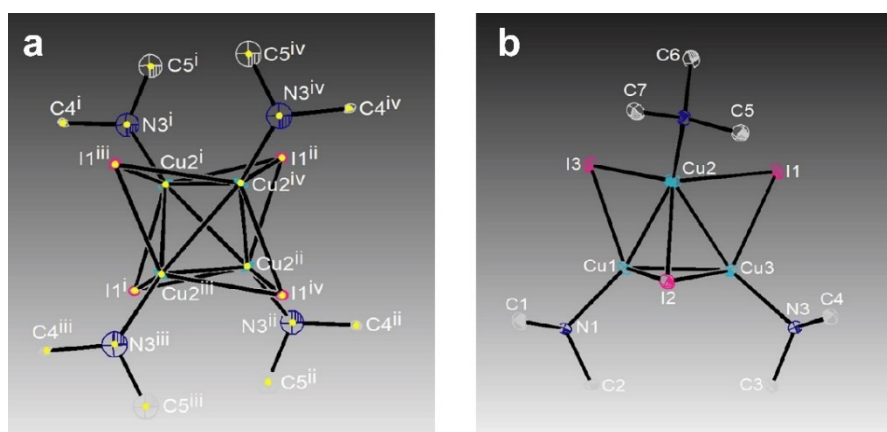


**Figure S2.** ORTEP drawing of a) $Cu_4I_4(Pip)_2$ b) $Cu_4I_4(DABCO)_2$ with 50% probability, H atoms have been omitted for clarity.

**Table S1:** Bond distance of the atoms

| Bond | $Cu_4I_4(Pip)_2$ | $Cu_4I_4(DABCO)_2$ |
|---|---|---|
| Cu-I | 2.636 – 2.751 Å | 2.631 – 2.751 Å |
| Cu-Cu | 2.617– 2.709 Å | 2.555 – 2.690 Å |
| Cu-N | 2.041 Å | 2.064 - 2.081 Å |
| C-N | 1.467– 1.481 Å | 1.479 – 1.497 Å |
| C-C | 1.49 - 1.50 Å | 1.54 Å |
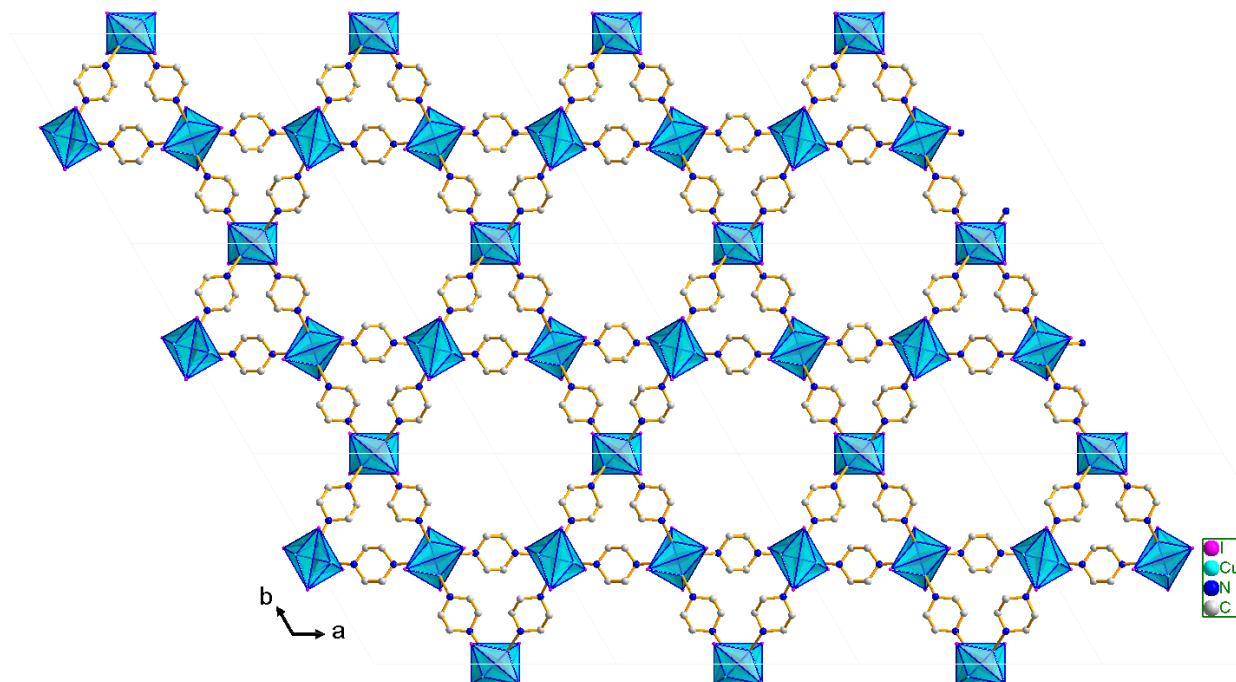
**Figure S3.** The 3D crystal structure of $Cu_4I_4(Pip)_2$. Colour scheme: $Cu_4I_4$: polyhedral (Cu: Cyan, I: Pink), N: Blue, C: Grey. Hydrogen atoms are omitted for clarity.
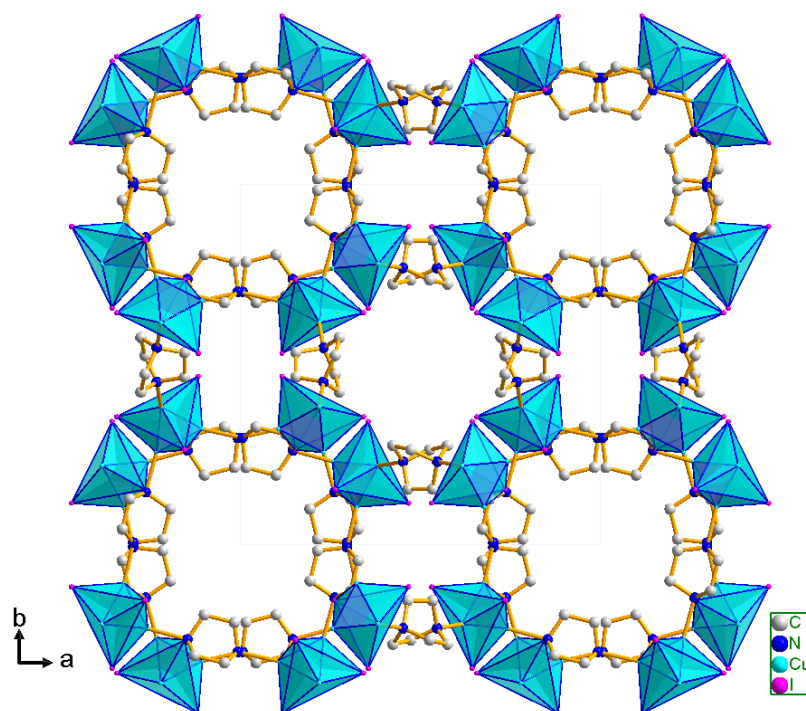


**Figure S4.** The 3D crystal structure of $Cu_4I_4(DABCO)_2$. Colour scheme: $Cu_4I_4$: polyhedral (Cu: Cyan, I: Pink), N: Blue, C: Grey. Hydrogen atoms are omitted for clarity.

# Section S-4: Powder X-ray Diffraction (PXRD) analysis
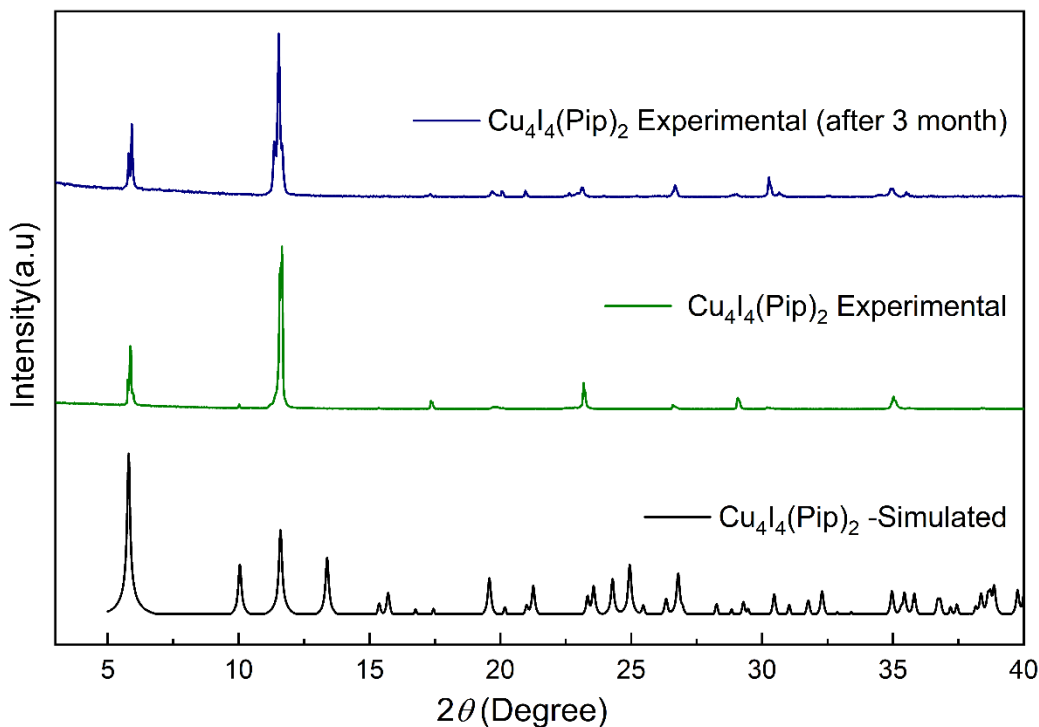


**Figure S5:** A comparison of powder X-ray diffraction (PXRD) data of freshly prepared $Cu_4I_4(Pip)_2$ (Green line), a three-month-old sample of $Cu_4I_4(Pip)_2$ (blue line) stored under ambient laboratory conditions, and the simulated profile obtained for $Cu_4I_4(Pip)_2$ (black line).

The powder X-ray diffraction (PXRD) data of more than three months old $Cu_4I_4(Pip)_2$ MOF crystals were kept in our laboratory under ambient conditions. The major peaks of the recorded data matched with that of freshly synthesized $Cu_4I_4(Pip)_2$ MOF and the simulated data generated from a single crystal file (CIF). This result signifies that $Cu_4I_4(Pip)_2$ MOF maintains its structural integrity under ambient conditions for at least three months.

# Section S-5: Fourier Transform Infrared (FT-IR) spectra analysis
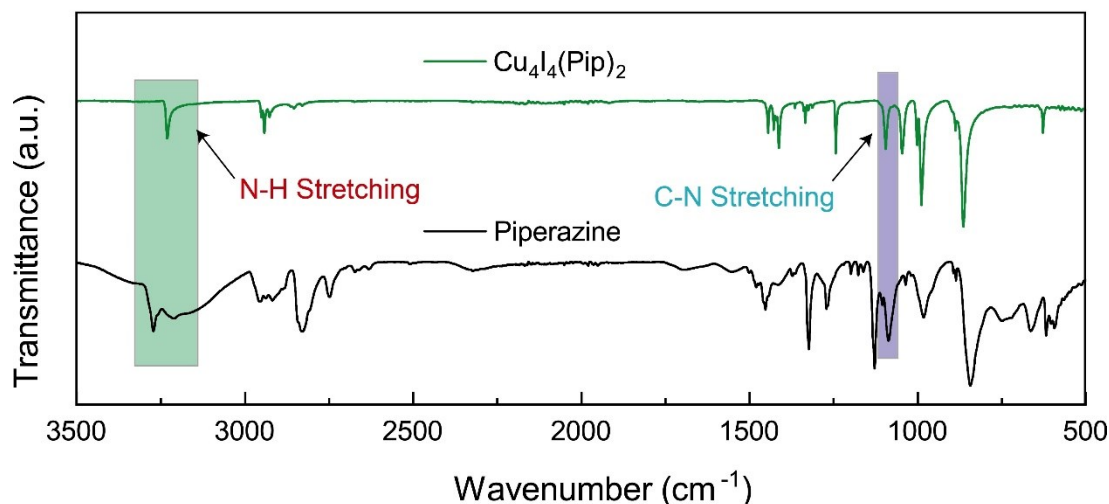


**Figure S6.** Comparison of FT-IR spectra of $Cu_4I_4(Pip)_2$ with the starting material piperazine.
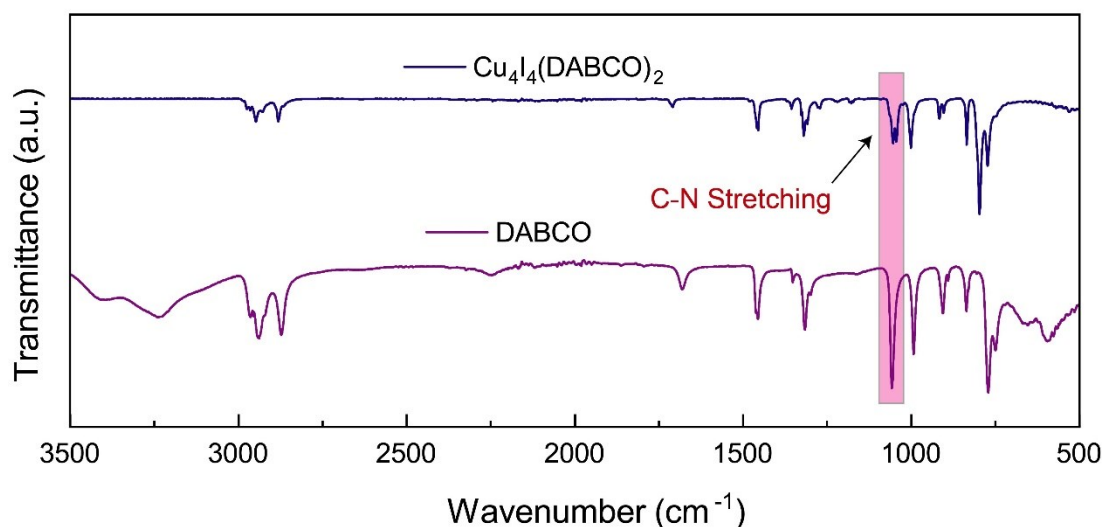


**Figure S7.** Comparison of FT-IR spectra of $Cu_4I_4(DABCO)_2$ with the starting material DABCO.

The successful synthesis of $Cu_4I_4(Pip)_2$ and $Cu_4I_4(DABCO)_2$ has been analyzed by FT-IR spectroscopy. The comparison FT-IR Spectra between piperazine and $Cu_4I_4(Pip)_2$ reveals shifts in the stretching frequency of the N-H from 3277 $cm^{-1}$ to 3234 $cm^{-1}$ and for C-N bonds from 1127 $cm^{-1}$ to 1090 $cm^{-1}$ after coordination with a Cu. There was a slight change in the C-N stretching frequency in case of $Cu_4I_4(DABCO)_2$ from 1056 $cm^{-1}$ to 1047 $cm^{-1}$. The shifts in the stretching frequency of N-H and C-N confirmed that there was a coordination bond between the copper atom of the cubane core and the N atom of the ligand.

# Section S-6: UV-Vis DRS and band gap analysis
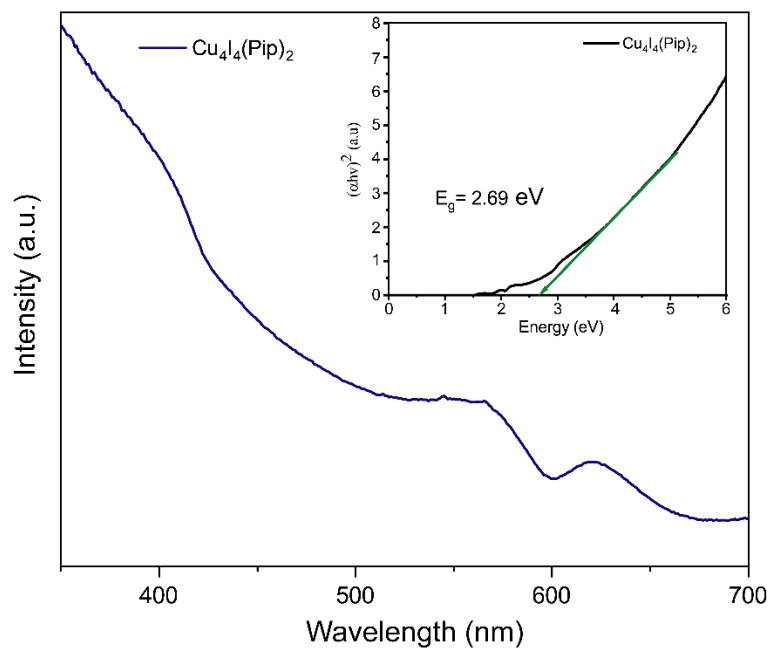


**Figure S8.** UV-vis diffuse reflectance spectroscopy and *Tauc* plot (inset) of Cu₄I₄(Pip)₂.
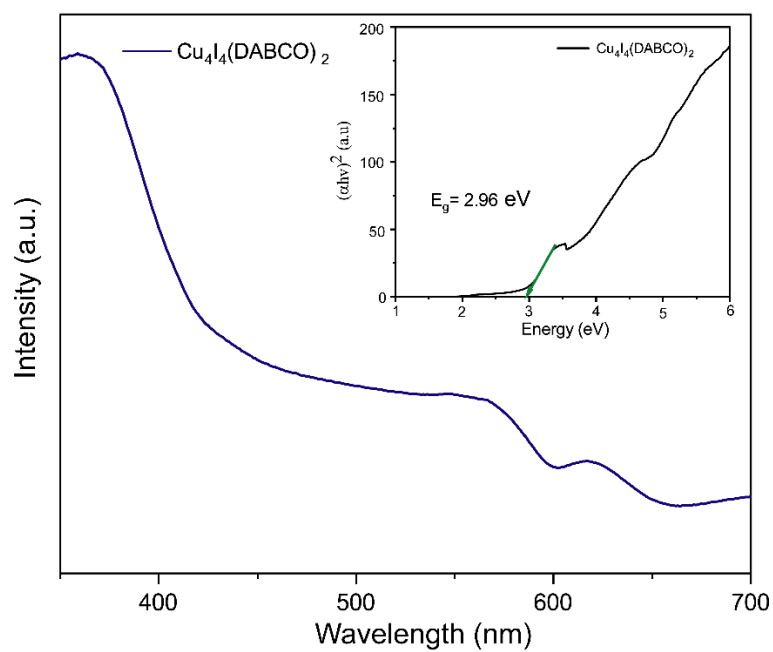


**Figure S9.** UV-vis diffuse reflectance spectroscopy and *Tauc* plot (inset) of Cu₄I₄(DABCO)₂.

**Table S2.** Absorbance peak and band gap calculation from UV-Vis DRS spectroscopy.

| Sl No. | Sample | Absorbance Peak (nm) | Band Gap (eV) |
|--------|--------|----------------------|---------------|
| 1. | $Cu_4I_4(Pip)_2$ | 407, 566, 622 | 2.69 |
| 2. | $Cu_4I_4(DABCO)_2$ | 360, 566, 616 | 2.96 |

The electronic band structure of $Cu_4I_4(Pip)_2$ and $Cu_4I_4(DABCO)_2$ was analyzed using UV-vis diffuse reflectance spectroscopy (DRS). For $Cu_4I_4(Pip)_2,$ the DRS spectra displayed absorbance peaks at 407, 566, and 622 nm, while $Cu_4I_4(DABCO)_2$, the DRS spectra exhibited absorbance peaks at 360, 566, and 616 nm, respectively, indicating the distinct absorption peak of both the compound.

From the Kubelka-munk transformation of the spectra, the band gap of $Cu_4I_4(Pip)_2$ and $Cu_4I_4(DABCO)_2$ was calculated to be 2.69 and 2.96 eV, respectively.

# Section S-7: Optical images of MOF crystals
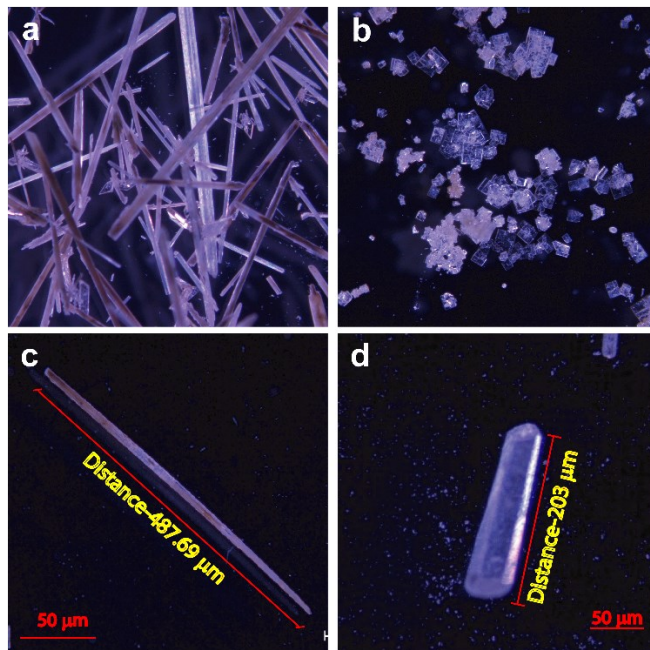


**Figure S10.** a,c) Optical images of $Cu_4I_4(Pip)_2$ and b,d) $Cu_4I_4(DABCO)_2$ crystals.
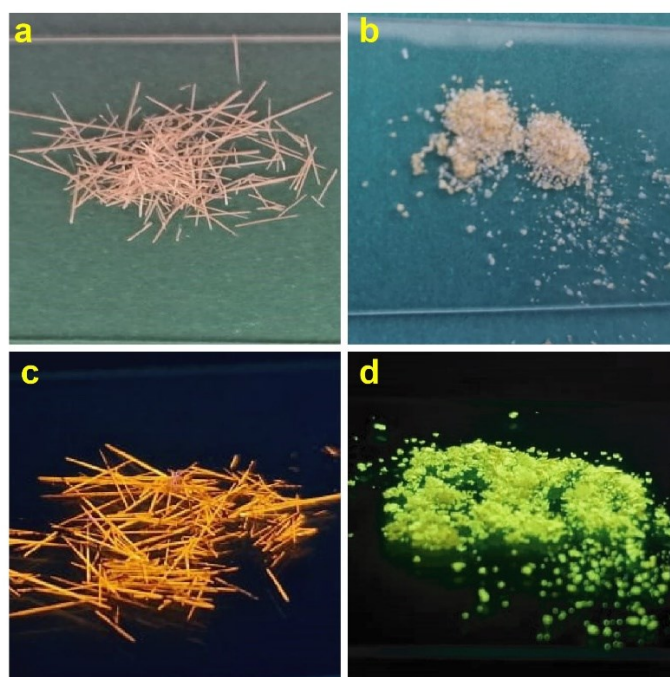


**Figure S11.** a,c) Optical images of $Cu_4I_4(Pip)_2$ and b,d) $Cu_4I_4(DABCO)_2$ crystals in naked eyes and under a UV light ($\lambda$=365 nm) respectively.

# Section S-8: Scanning electron microscopy (SEM)
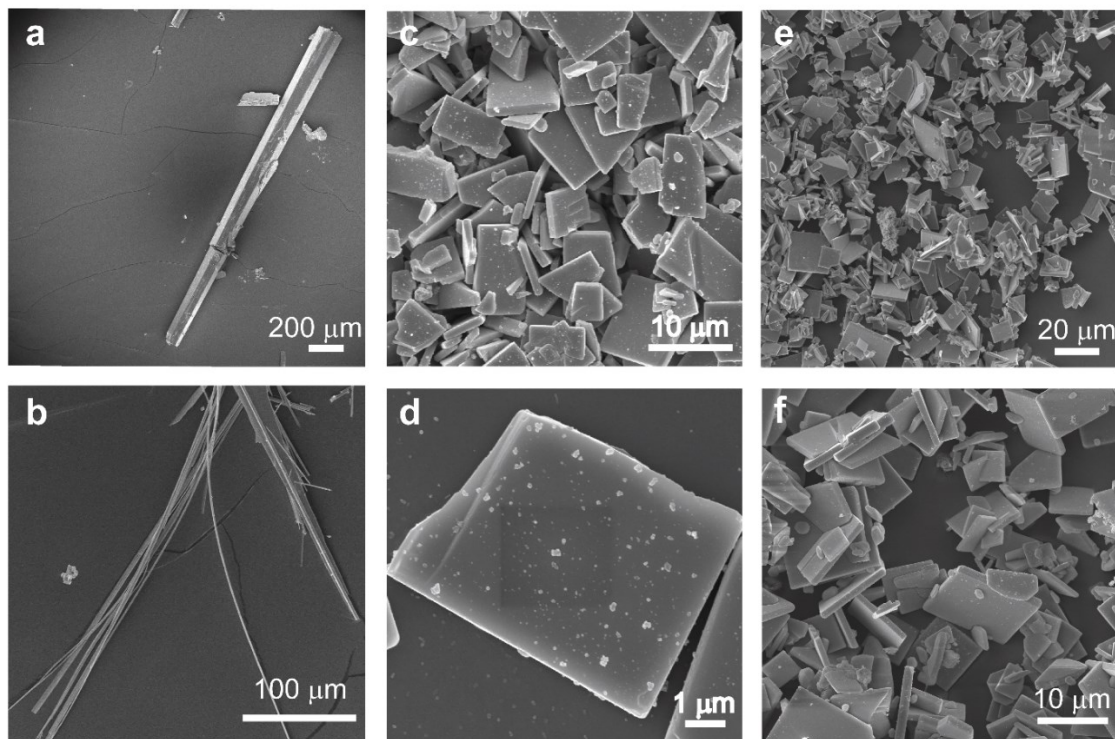


**Figure S12.** SEM images of a-b) $Cu_4I_4(Pip)_2$ crystals; c-d) $Cu_4I_4(DABCO)_2$ crystals and e-f) $Cu_4I_4(DABCO)_2$ powders.

The surface morphology of all the synthesized materials was examined by SEM. The SEM images of the $Cu_4I_4(Pip)_2$ show needle-like morphology. On the other hand, $Cu_4I_4(DABCO)_2$ exhibits uniform block-like morphology.
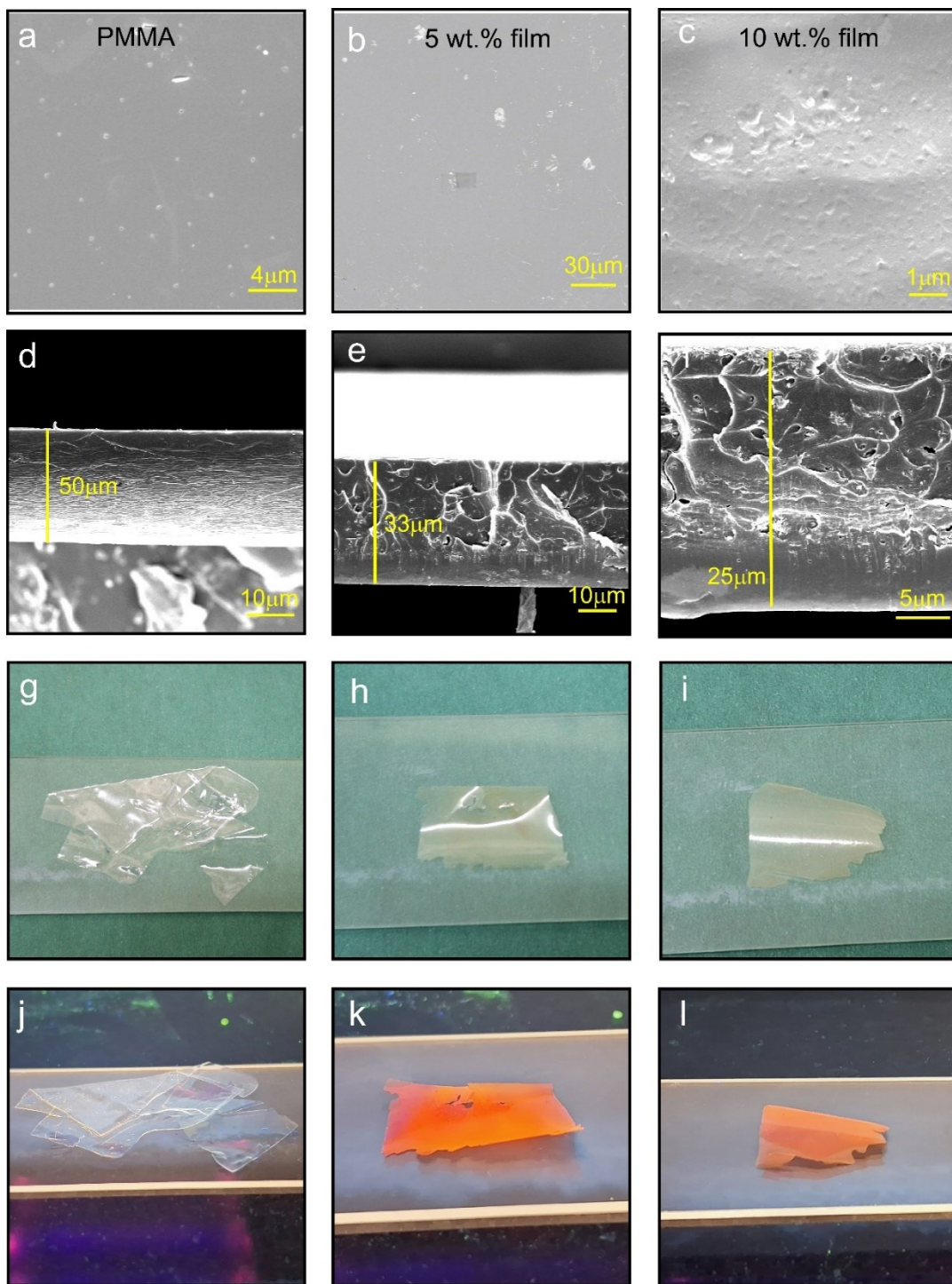
**Figure S13**: SEM images, cross-section, digital image and under UV-light ($\lambda$=365 nm): (a,d,g,j) PMMA; (b,e,h,k) 5 wt.% and (c,f,i,l) 10 wt.% composite film of PMMA-Cu$_4$I$_4$(Pip)$_2$, respectively.

# Section S-9: Thermochemical stability
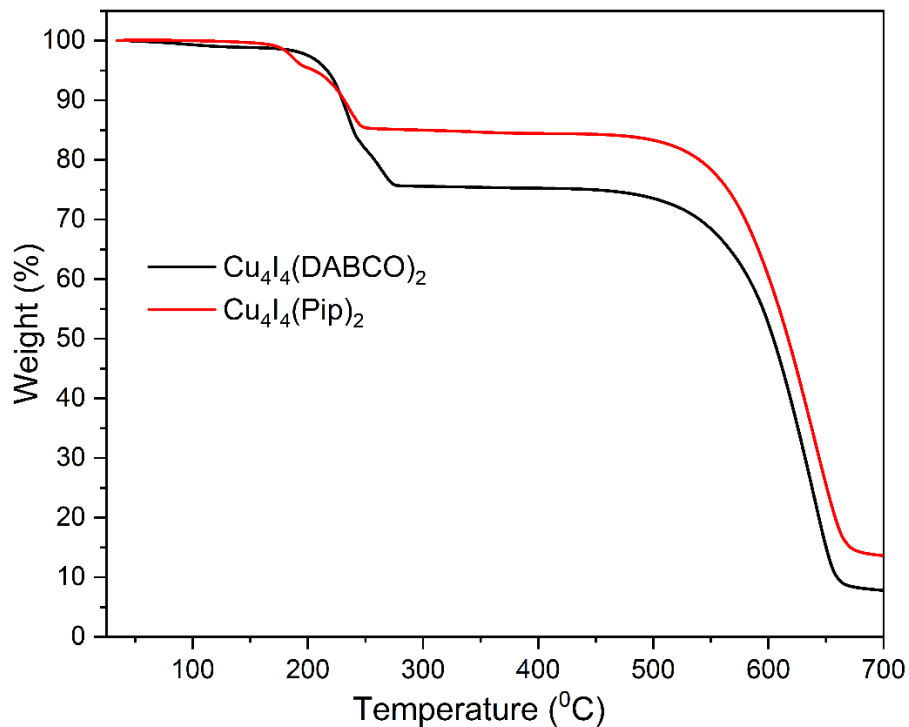


**Figure S14.** Thermogravimetric analysis (TGA) profiles of $Cu_4I_4(DABCO)_2$ and $Cu_4I_4(Pip)_2$ crystals.
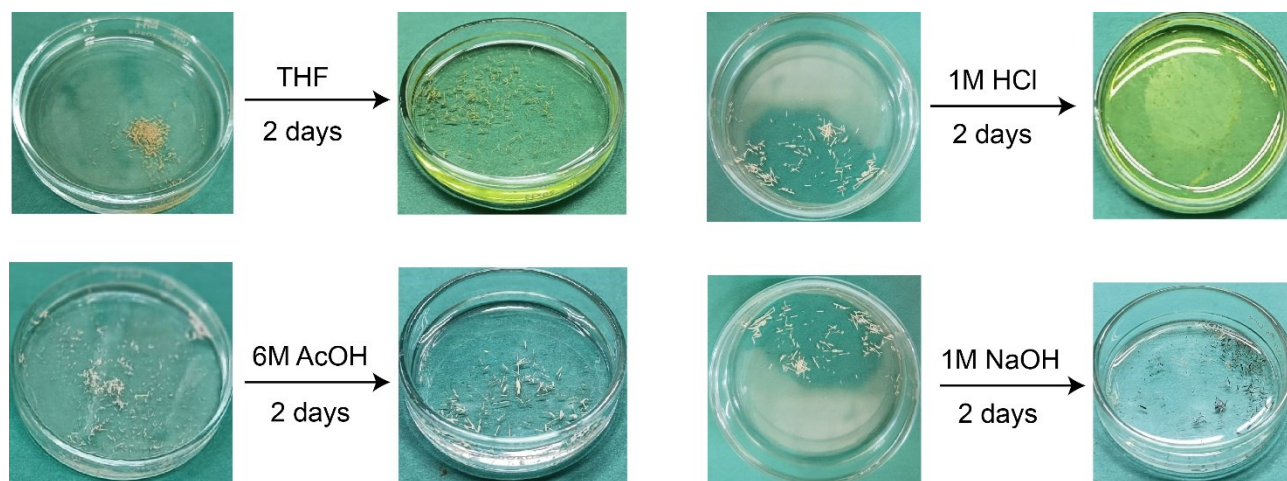


**Figure S15.** Chemical stability study of $Cu_4I_4(Pip)_2$ crystals in various conditions. The crystals were stable in common organic solvents and in mild acidic conditions (6M Acetic acid). However, the MOF crystals were degraded in acidic (1M HCl) or basic (1M NaOH) conditions.

## Section S-10: N₂ sorption studies
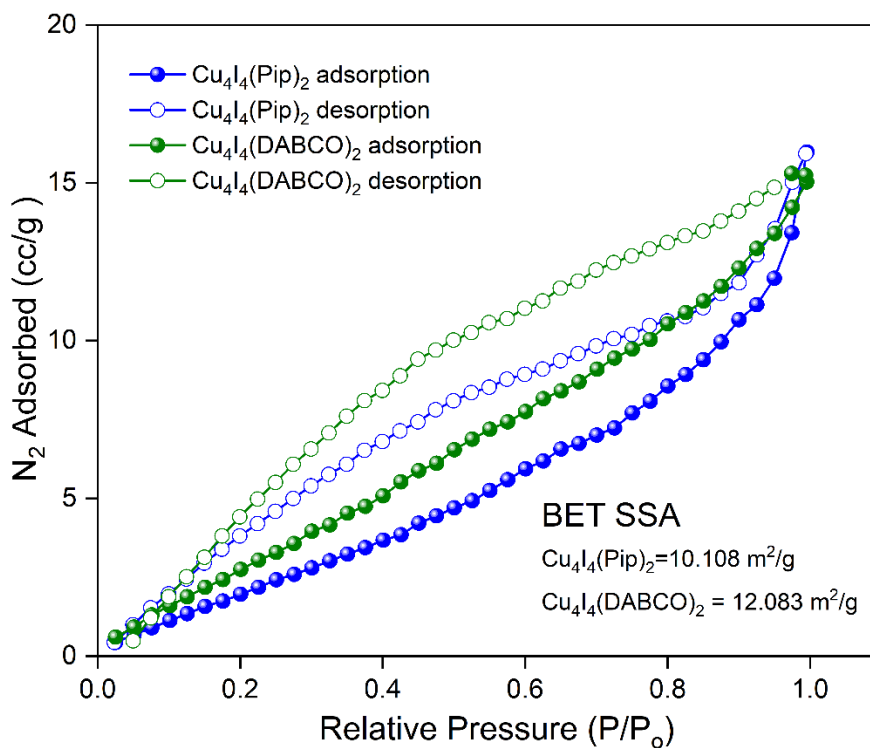


**Figure S16.** $N_2$ sorption isotherm for $Cu_4I_4(DABCO)_2$ and $Cu_4I_4(Pip)_2$ MOFs at 77 K. The Brunauer–Emmett–Teller (BET) surface area of $Cu_4I_4(DABCO)_2$ and $Cu_4I_4(Pip)_2$ were calculated to be 12 $m^2g^{-1}$ and 10. $m^2g^{-1}$, respectively.
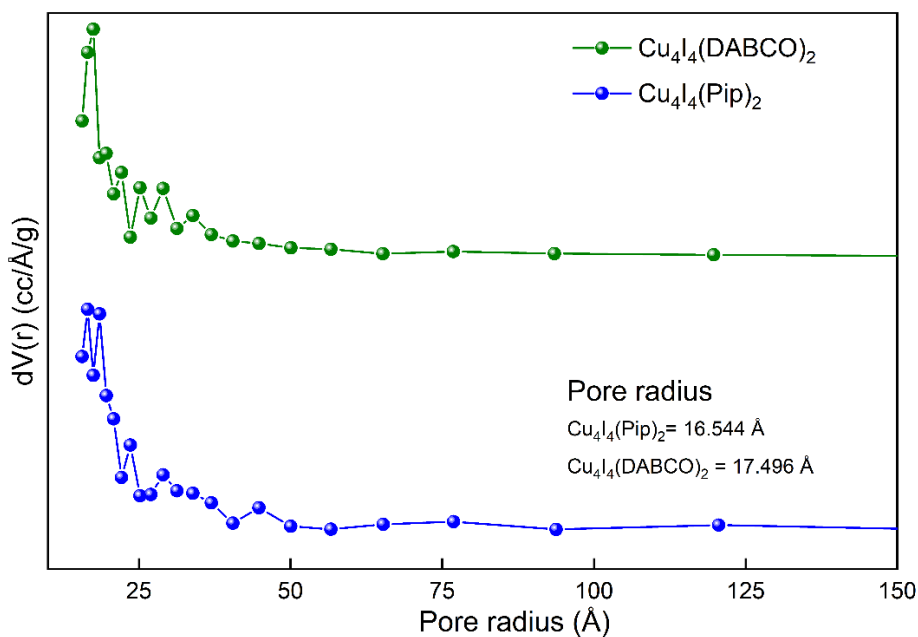


**Figure S17.** Pore size distribution plot of $Cu_4I_4(DABCO)_2$ and $Cu_4I_4(Pip)_2$ MOFs, obtained from the $N_2$ sorption studies at 77 K using non-local density functional theory (NLDFT) pore size analysis method.

## Section S-11: Piezoelectric studies
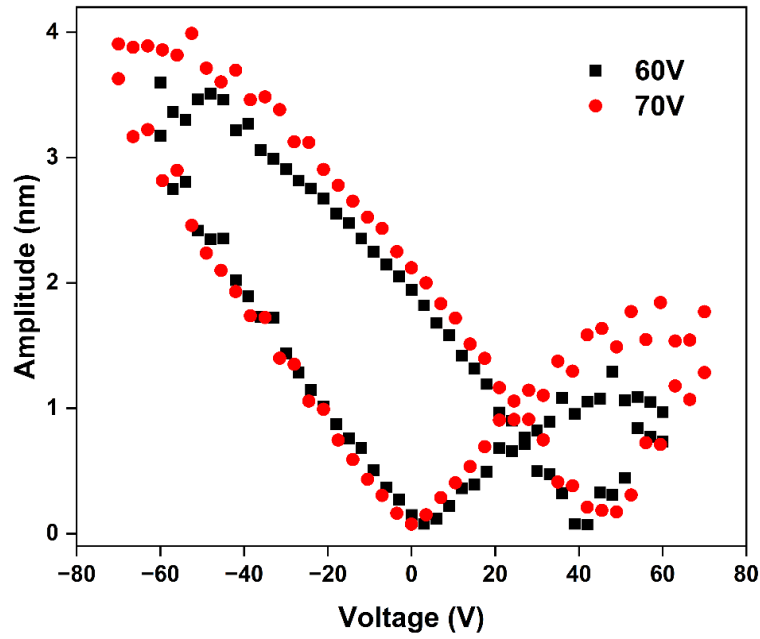


**Figure S18.** Amplitude changes with variation of the voltage in SS-PFM at 60V and 70V in region 1.
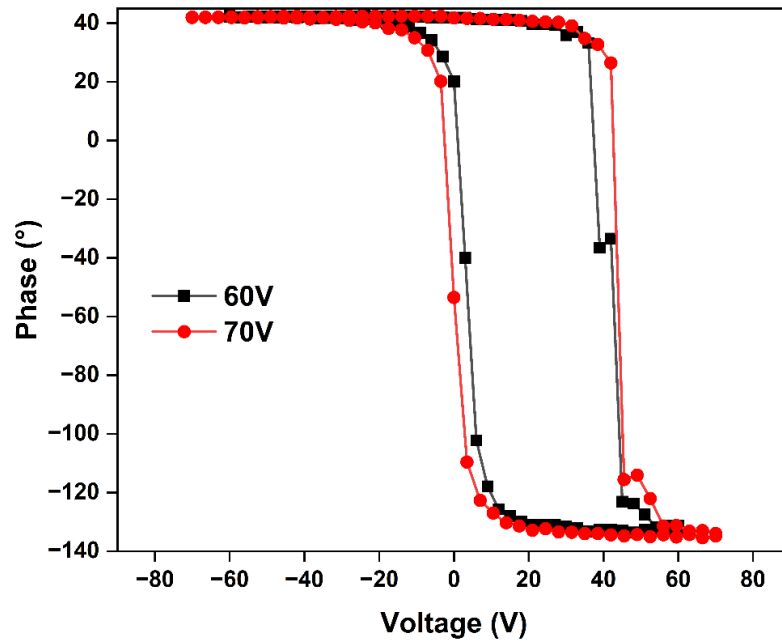


**Figure S19.** Phase changes with variation of the voltage in SS-PFM at 60V and 70V in region 1.
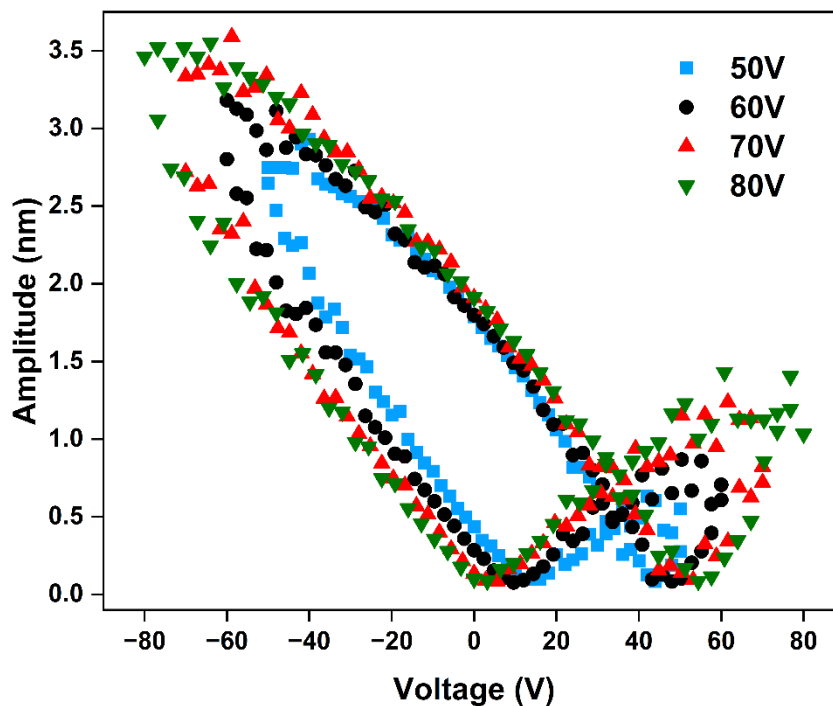
**Figure S20.** Amplitude changes with variation of the voltage in SS-PFM at 50V, 60V, 70V, and 80V in region 2.
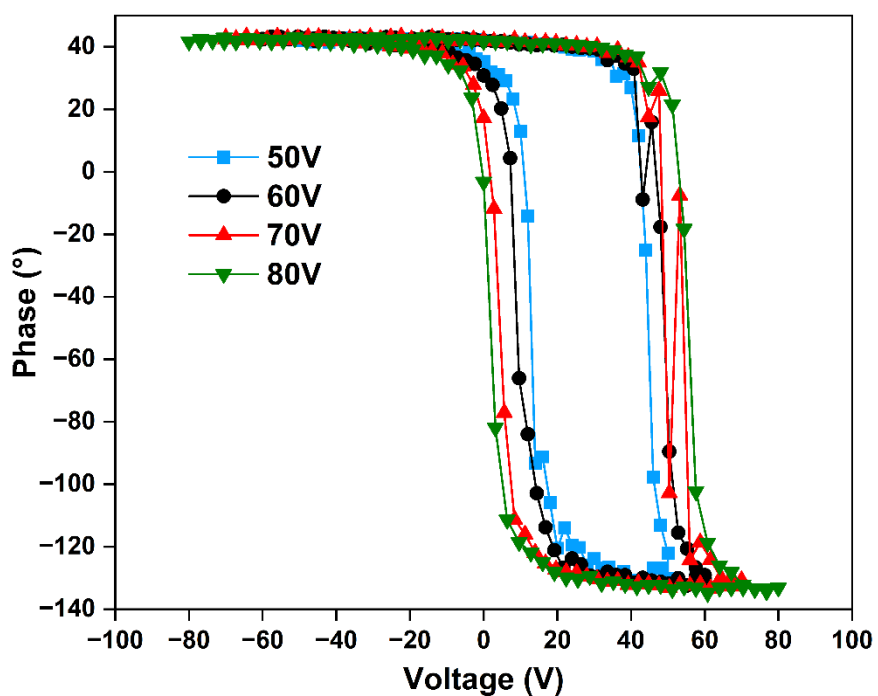


**Figure S21.** Phase changes with variation of the voltage in SS-PFM at 50V, 60V, 70V, and 80V in region 2.

85.8 nm

-21.6 nm

79.6 nm

-20.4 nm

87.1 nm

-21.5 nm
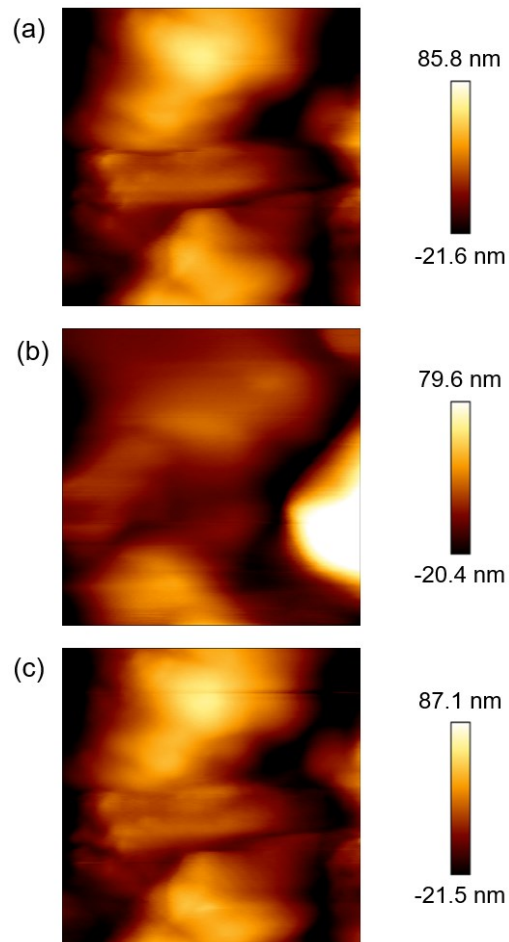
**Figure S22.** Topography under application of (a) -10V, (b) 0V, and (c) +10V corresponding to Figure 2 (main manuscript).
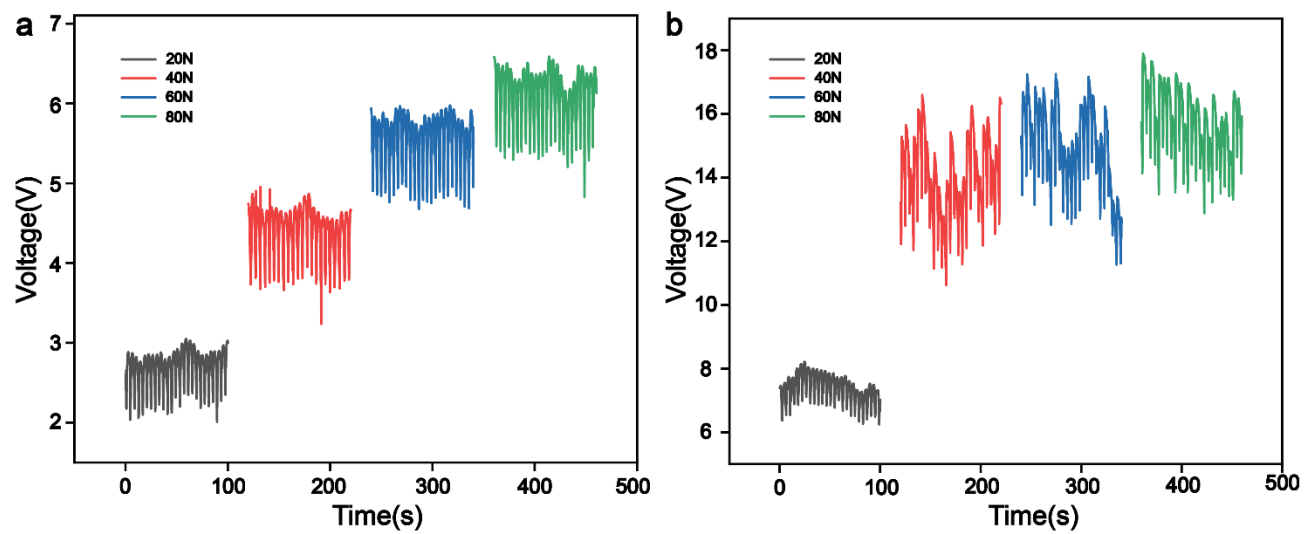


**Figure S23.** Force-dependent voltage harvesting measurements for (a) 5 wt% (b) 10 wt % $Cu_4I_4(Pip)_2$-PMMA film [3 months old $Cu_4I_4(Pip)_2$].

**Table S3:** Comparison of piezoelectric MOFs and their piezoelectric coefficient ($d_{33}$).

| Sl NO. | Materials | Piezoelectric coefficient ($d_{33}$) (pm/V) | Ref. |
|---|---|---|---|
| 1. | NUS-6-(Zr); NUS-6-(Hf) | 1.5-2.5; 2.0-3.5 | S4 |
| 2. | AlN; InN | 5.4; 7.6 | S5 |
| 3. | CdS | 10.32 | S6 |
| 4. | PVDF | 10-20 | S7 |
| 5. | $MAPbI_3$ | 10.81 | S8 |
| 6. | GaN | 12.4 | S9 |
| 7. | MDABCO-$NH_4I_3$ | 12.8 | S10 |
| 8. | ZnO | 14.3-26.7 | S11 |
| 9. | GaAs | 26 | S12 |
| 10. | P(VDF-TrFe) | 25-45 | S13 |
| 11. | PMN-PT | 50 | S14 |
| 12. | **$Cu_4I_4(Pip)_2$** | **52.3** | **This Work** |
| 13. | UiO-66-$NH_2$ | 62 | S15 |
| 14. | UiO-66 | 71 | S16 |
| 15. | $CsPb_2Br_5$ | 72 | S17 |
| 16. | MIL-53(Cr) | 100 | S15 |
| 17. | $LiNbO_3$ | 100 | S18 |
| 18. | PZT | 127 | S19 |

**Table S4:** Crystallographic data table for $Cu_4I_4(Pip)_2$.

| | |
|---|---|
| Empirical formula | $C_2 H_5 Cu I N$ |
| Formula weight | 233.51 |
| T (K)/$\lambda$ (Å) | 113(19) |
| Crystal system | Hexagonal |
| Space group | $P6_222$ |
| $a$ (Å) | 17.5937(5) |
| $b$ (Å) | 17.5937(5) |
| $c$ (Å) | 7.3368(2) |
| $\alpha$ (°) | 90 |
| $\beta$ (°) | 90 |
| $\gamma$ (°) | 120 |
| Volume ($Å^3$) | 1966.76(12) |
| Z | 12 |
| $\rho_{calcd}$ (g cm$^{-3}$) | 2.366 |
| $\mu$ (mm$^{-1}$) | 40.590 |
| F(000) | 1272.0 |
| Crystal size/ mm$^3$ | $0.2 \times 0.2 \times 0.1$ |
| Radiation | Cu K$\alpha$ ($\lambda$ = 1.54184) |
| 2θ range for data collection | 10.056 to 155.49 |
| Index ranges | $-21 \leq h \leq 21, -22 \leq k \leq 22, -8 \leq l \leq 4$ |
| Reflections collected | 7796 |
| Independent reflections | 1384 [$R_{int}$ = 0.0726, $R_{sigma}$ = 0.0324] |
| Data/restraints/parameter | 1384/0/46 |
| Goodness-of-fit on $F^2$ | 1.167 |
| Final R indexes [I >= 2σ(I)] | 0.0539/0.1563 |
| Final R indexes (all data) | 0.0551/0.1589 |
| largest diff. peak/hole (e Å$^{-3}$) | 2.31/-1.87 |

**Table S5:** Crystallographic data table for $Cu_4I_4(DABCO)_2$.

| | |
|---|---|
| Empirical formula | $C_{12}H_{24}Cu_4I_4N_4$ |
| Formula weight | 986.11 |
| T (K)/$\lambda$ (Å) | 80(2) |
| Crystal system | Tetragonal |
| Space group | $P4/mcc$ |
| $a$ (Å) | 17.9914(2) |
| $b$ (Å) | 17.9914(2) |
| $c$ (Å) | 15.9344(3) |
| $\alpha$ (°) | 90 |
| $\beta$ (°) | 90 |
| $\gamma$ (°) | 90 |
| Volume ($Å^3$) | 5157.81(13) |
| Z | 8 |
| $\rho_{calcd}$ (g $cm^{-3}$) | 2.540 |
| $\mu$ ($mm^{-1}$) | 8.045 |
| F(000) | 3616.0 |
| Crystal size/ $mm^3$ | $0.2 \times 0.2 \times 0.1$ |
| Radiation | MoK$\alpha$ ($\lambda$ = 0.71073) |
| 2θ range for data collection | 5.06 to 57.68 |
| Index ranges | $-22 \leq h \leq 21, -22 \leq k \leq 23, -21 \leq l \leq 11$ |
| Reflections collected | 15432 |
| Independent reflections | 3224 [$R_{int}$ = 0.0277, $R_{sigma}$ = 0.0239] |
| Data/restraints/parameter | 3224/0/122 |
| Goodness-of-fit on $F^2$ | 1.088 |
| Final R indexes [I >= 2σ(I)] | 0.0278/0.0553 |
| Final R indexes (all data) | 0.0378/0.0574 |
| largest diff. peak/hole (e $Å^{-3}$) | 1.09/-0.76 |

**Table S6:** Bond lengths for Cu$_4$I$_4$(Pip)$_2$.

| Atom | Atom | Length/Å | Atom | Atom | Length/Å |
|------|------|----------|------|------|----------|
| I1 | Cu2 | 2.636(2) | Cu2 | Cu2$^3$ | 2.617(4) |
| I1 | Cu2$^1$ | 2.751(2) | Cu2 | N3 | 2.041(12) |
| I1 | Cu2$^2$ | 2.691(2) | N3 | C5 | 1.467(18) |
| Cu2 | I1$^2$ | 2.691(2) | N3 | C4 | 1.481(18) |
| Cu2 | I1$^1$ | 2.751(2) | C5 | C5$^4$ | 1.49(3) |
| Cu2 | Cu2$^2$ | 2.709(4) | C4 | C4$^4$ | 1.50(3) |

**Table S7:** Bond lengths for Cu$_4$I$_4$(DABCO)$_2$.

| Atom | Atom | Length/Å | Atom | Atom | Length/Å |
|------|------|----------|------|------|----------|
| C1 | C4$^1$ | 1.542(5) | N3 | Cu3 | 2.064(5) |
| C1 | N1 | 1.484(5) | Cu1 | Cu2$^5$ | 2.6490(7) |
| C2 | C3$^2$ | 1.547(8) | Cu1 | Cu2 | 2.6490(7) |
| C2 | N1 | 1.489(7) | Cu1 | Cu3 | 2.5551(10) |
| C3 | C2$^3$ | 1.547(8) | Cu1 | I2$^5$ | 2.7213(4) |
| C3 | N3 | 1.483(7) | Cu1 | I2 | 2.7213(4) |
| C4 | C1$^3$ | 1.542(5) | Cu1 | I3 | 2.6704(8) |
| C4 | N3 | 1.486(5) | Cu2 | Cu2$^5$ | 2.6727(10) |
| C5 | C5$^4$ | 1.529(8) | Cu2 | Cu3 | 2.6900(8) |
| C5 | N2 | 1.497(5) | Cu2 | I1 | 2.7514(6) |
| C6 | C7$^4$ | 1.548(6) | Cu2 | I2 | 2.6513(6) |
| C6 | N2 | 1.495(5) | Cu2 | I3 | 2.6311(6) |
| C7 | C6$^4$ | 1.548(6) | Cu3 | Cu2$^5$ | 2.6900(8) |
| C7 | N2 | 1.479(5) | Cu3 | I1 | 2.6322(8) |
| N2 | Cu2 | 2.081(3) | Cu3 | I2 | 2.6947(4) |
| N1 | C1$^5$ | 1.484(5) | Cu3 | I2$^5$ | 2.6947(4) |
| N1 | Cu1 | 2.065(4) | I1 | Cu2$^5$ | 2.7514(6) |
| N3 | C4$^5$ | 1.486(5) | I3 | Cu2$^5$ | 2.6311(6) |

**Table S8:** Bond angles for $Cu_4I_4(Pip)_2$.

| Atom | Atom | Atom | Angle/° | Atom | Atom | Atom | Angle/° |
|------|------|------|---------|------|------|------|---------|
| Cu2 | I1 | Cu2$^1$ | 61.12(8) | Cu2$^2$ | Cu2 | Cu2$^1$ | 58.71(9) |
| Cu2 | I1 | Cu22 | 58.34(8) | Cu2$^3$ | Cu2 | Cu2$^2$ | 62.20(9) |
| Cu2$^1$ | I1 | Cu2$^2$ | 57.48(8) | Cu2$^3$ | Cu2 | Cu2$^1$ | 59.09(9) |
| I1 | Cu2 | I1$^1$ | 106.29(8) | N3 | Cu2 | I1$^1$ | 104.9(4) |
| I1 | Cu2 | I1$^2$ | 115.27(8) | N3 | Cu2 | I1 | 110.6(4) |
| I11 | Cu2 | I12 | 118.02(8) | N3 | Cu2 | I1$^2$ | 101.1(4) |
| I1 | Cu2 | Cu2$^1$ | 60.44(7) | N3 | Cu2 | Cu2$^1$ | 152.3(4) |
| I11 | Cu2 | Cu2$^1$ | 58.44(8) | N3 | Cu2 | Cu2$^3$ | 136.7(3) |
| Cu2$^3$ | Cu2 | I1$^2$ | 60.11(8) | N3 | Cu2 | Cu2$^2$ | 144.4(4) |
| Cu2$^2$ | Cu2 | I1$^1$ | 110.54(5) | C5 | N3 | Cu2 | 112.7(9) |
| Cu2$^1$ | Cu2 | I1$^2$ | 106.38(5) | C5 | N3 | C4 | 109.8(12) |
| Cu2$^3$ | Cu2 | I1 | 112.63(5) | C4 | N3 | Cu2 | 117.7(10) |
| Cu2$^2$ | Cu2 | I1$^2$ | 58.65(8) | N3 | C5 | C5$^4$ | 114.3(11) |
| Cu2$^3$ | Cu2 | I1$^1$ | 62.41(9) | N3 | C4 | C4$^4$ | 114.7(11) |
| Cu2$^2$ | Cu2 | I1 | 63.01(8) | | | | |

**Table S9:** Bond Angles for $Cu_4I_4(DABCO)_2$.

| Atom | Atom | Atom | Angle/° | Atom | Atom | Atom | Angle/° |
|---|---|---|---|---|---|---|---|
| N1 | C1 | C4[1] | 111.0(3) | N2 | Cu2 | I1 | 97.06(9) |
| N1 | C2 | C3[2] | 110.3(5) | N2 | Cu2 | I2 | 103.44(9) |
| N3 | C3 | C2[3] | 111.1(4) | N2 | Cu2 | I3 | 115.80(9) |
| N3 | C4 | C1[3] | 110.6(4) | Cu1 | Cu2 | Cu2[5] | 59.704(13) |
| N2 | C5 | C5[4] | 109.9(2) | Cu1 | Cu2 | Cu3 | 57.18(2) |
| N2 | C6 | C7[4] | 110.6(3) | Cu1 | Cu2 | I1 | 106.54(2) |
| N2 | C7 | C6[4] | 109.9(3) | Cu1 | Cu2 | I2 | 61.783(16) |
| C5 | N2 | Cu2 | 106.8(2) | Cu2[5] | Cu2 | Cu3 | 60.212(13) |
| C6 | N2 | C5 | 108.6(3) | Cu2[5] | Cu2 | I1 | 60.941(11) |
| C6 | N2 | Cu2 | 110.9(3) | Cu3 | Cu2 | I1 | 57.846(19) |
| C7 | N2 | C5 | 106.2(3) | I2 | Cu2 | Cu2[5] | 111.948(12) |
| C7 | N2 | C6 | 107.0(3) | I2 | Cu2 | Cu3 | 60.592(16) |
| C7 | N2 | Cu2 | 117.0(2) | I2 | Cu2 | I1 | 109.01(2) |
| C15 | N1 | C1 | 107.6(5) | I3 | Cu2 | Cu1 | 60.760(19) |
| C1 | N1 | C2 | 108.5(3) | I3 | Cu2 | Cu2[5] | 59.475(12) |
| C15 | N1 | C2 | 108.5(3) | I3 | Cu2 | Cu3 | 108.13(2) |
| C15 | N1 | Cu1 | 111.6(2) | I3 | Cu2 | I1 | 115.34(2) |
| C1 | N1 | Cu1 | 111.6(2) | I3 | Cu2 | I2 | 114.32(2) |
| C2 | N1 | Cu1 | 109.0(3) | N3 | Cu3 | Cu1 | 140.00(13) |
| C3 | N3 | C4 | 108.2(3) | N3 | Cu3 | Cu2 | 146.73(6) |
| C3 | N3 | C4[5] | 108.2(3) | N3 | Cu3 | Cu2[5] | 146.73(6) |
| C3 | N3 | Cu3 | 109.7(3) | N3 | Cu3 | I1 | 106.89(13) |
| C4[5] | N3 | C4 | 108.2(4) | N3 | Cu3 | I2 | 103.18(6) |
| C4[5] | N3 | Cu3 | 111.3(2) | N3 | Cu3 | I25 | 103.18(6) |
| C4 | N3 | Cu3 | 111.3(2) | Cu1 | Cu3 | Cu2[5] | 60.60(2) |
| N1 | Cu1 | Cu2[5] | 148.25(4) | Cu1 | Cu3 | Cu2 | 60.60(2) |
| N1 | Cu1 | Cu2 | 148.25(4) | Cu1 | Cu3 | I1 | 113.11(3) |
| N1 | Cu1 | Cu3 | 132.66(13) | Cu1 | Cu3 | I2 | 62.377(14) |

| Atom | Atom | Atom | Angle/° | Atom | Atom | Atom | Angle/° |
|---|---|---|---|---|---|---|---|
| N1 | Cu1 | I2 | 100.44(7) | Cu1 | Cu3 | I2$^{5}$ | 62.377(14) |
| N1 | Cu1 | I25 | 100.44(7) | Cu2$^{5}$ | Cu3 | Cu2 | 59.58(3) |
| N1 | Cu1 | I3 | 116.27(13) | Cu2$^{5}$ | Cu3 | I2 | 110.06(3) |
| Cu2$^{5}$ | Cu1 | Cu2 | 60.59(3) | Cu2$^{5}$ | Cu3 | I2$^{5}$ | 58.994(15) |
| Cu2 | Cu1 | I2 | 59.149(15) | Cu2 | Cu3 | I2$^{5}$ | 110.06(3) |
| Cu2$^{5}$ | Cu1 | I2$^{5}$ | 59.149(15) | Cu2 | Cu3 | I2 | 58.994(15) |
| Cu2$^{5}$ | Cu1 | I2 | 110.49(3) | I1 | Cu3 | Cu2$^{5}$ | 62.247(19) |
| Cu2 | Cu1 | I25 | 110.49(3) | I1 | Cu3 | Cu2 | 62.247(19) |
| Cu2 | Cu1 | I3 | 59.288(18) | I1 | Cu3 | I2 | 111.336(16) |
| Cu2$^{5}$ | Cu1 | I3 | 59.288(18) | I1 | Cu3 | I2$^{5}$ | 111.336(16) |
| Cu3 | Cu1 | Cu2 | 62.22(2) | I2$^{5}$ | Cu3 | I2 | 119.46(3) |
| Cu3 | Cu1 | Cu2$^{5}$ | 62.22(2) | Cu2$^{5}$ | I1 | Cu2 | 58.12(2) |
| Cu3 | Cu1 | I2 | 61.326(14) | Cu3 | I1 | Cu2$^{5}$ | 59.906(17) |
| Cu3 | Cu1 | I2$^{5}$ | 61.326(14) | Cu3 | I1 | Cu2 | 59.906(17) |
| Cu3 | Cu1 | I3 | 111.06(3) | Cu2 | I2 | Cu1 | 59.068(18) |
| I2 | Cu1 | I2$^{5}$ | 117.57(3) | Cu2 | I2 | Cu3 | 60.414(19) |
| I3 | Cu1 | I2 | 110.803(17) | Cu3 | I2 | Cu1 | 56.297(19) |
| I3 | Cu1 | I2$^{5}$ | 110.803(17) | Cu2$^{5}$ | I3 | Cu1 | 59.952(17) |
| N2 | Cu2 | Cu1 | 155.13(10) | Cu2 | I3 | Cu1 | 59.952(17) |
| N2 | Cu2 | Cu2$^{5}$ | 142.69(9) | Cu2$^{5}$ | I3 | Cu2 | 61.05(2) |
| N2 | Cu2 | Cu3 | 135.76(9) | | | | |

Checkcif file A-level alerts which have been addressed as follows:

PLAT211_ALERT_2_A ADP of Atom N3 is N.P.D. or (nearly) 2D. Please Check.

PLAT211_ALERT_2_A ADP of Atom C5 is N.P.D. or (nearly) 2D. Please Check.

Note: The C5 and N3 atoms of the piperazine ring in $Cu_4I_4(Pip)_2$ showed the disorder due to the diffused electron density of these atoms in the measured crystal data, which in turn generated the alerts PLAT211_ALERT_2_A. However, this does not indicate any incorrect atom assignment.

PLAT601_ALERT_2_A Unit Cell Contains Solvent Accessible VOIDS of. 593 Ang**3

Note: The highest peak in the final difference map is just 2.2 e/A3. Therefore, no model for any solvent could be found.

# References

1. G. M. Sheldrick, Acta Crystallogr. *C. Struct Chem*, 2015, **71**, 3–8.

2. O. V. Dolomanov, L. J. Bourhis, R. J. Gildea, J. A. K. Howard, H. Puschmann, *J. Appl. Crystallogr.* 2009, **42**, 339-341.

3. (a) G. M. Sheldrick, *Crystallogr.* 2008, **64**, 112-122; (b) G. M. Sheldrick, *Acta Crystallogr. Sect. A*, 2015, **A71**, 3-8.

4. Y. Sun, Z. Hu, D. Zhao and K. Zeng, *Nanoscale,* 2017, **9**, 12163–12169.

5. F. Bernardini and V. Fiorentini, *Appl. Phys.*, 2002, **80**, 4145–4147.

6. D. Berlincourt; H. Jaffe, L. R. Shiozawa, *Phys. Rev.*, 1963, **129**, 1009–1017.

7. V. Cauda, B. Torre, A. Falqui, G. Canavese, S. Stassi, T. Bein and M. Pizzi., *Chem. Mater.*, 2012, **24**, 4215–4221.

8. Q. Lai, L. Zhu, Y. Pang, L. Xu, J. Chen, Z. Ren, J. Luo, L. Wang, L. Chen, K. Han, P. Lin, D. Li, S. Lin, B. Chen, C. Pan and Z. L. Wang. *ACS nano,* 2018, **12**, 10501–10508.

9. M. Minary-Jolandan, R. A. Bernal, I. Kuljanishvili, V. Parpoil and H. D. Espinosa, *Nano Lett.,* 2012, **12**, 970–976.

10. H. Wu, S. Wei, S. Chen, H. Pan, W. Pan, S. Huang, M. Tsai and P. Yang, *Adv. Sci.,* 2022, **9**, 2105974.

11. M.-H. Zhao, Z.-L. Wang and S. X. Mao, *Nano Lett,* 2004, **4**, 587–590.

12. P. A. Alekseev, V. A. Sharov, P. Geydt, M. S. Dunaevskiy, V. V. Lysak, G. E. Cirlin, R. R. Reznik, A. I. Khrebtov, I. P. Soshnikov and E. Lähderanta, *Phys. Status Solidi RRL,* 2017, **12**, 1700358.

13. Y. Wu, Q. Gu, G. Ding, F. Tong, Z. Hu and A. M. Jonas, *ACS Macro Lett.* 2013, **2**, 535–538.

14. S. Xu, G. Poirier and N. Yao. *Nano Energy,* 2012, **1**, 602–607.

15. R. Ding, Q. Liu and L. Zheng, *Chem. Eur. J.* 2023, **29**, e202203792.

16. L. Cai, J. Du, F. Han, T. Shi, H. Zhang, Y. Lu, S. Long, W. Sun, J. Fan and X. Peng, *ACS Nano,* 2023, **17**, 7901–7910.

17. A. Sahoo, T. Paul, N. H. Makani, S. Maiti, and R. Banerjee, *Sustain. Energ. Fuels*, 2022, **6**, 4484–4497.

18. Z. Chen, J. Huang, Y. Yang, Y. Wang, Y. Wu, H. He, X. Wei, Z. Ye, H. Zeng, H. Cong and Z. Jiang, *RSC Adv.,* 2012, **2**, 7380.

19. R. Steinhausen, T. Hauke, H. Beige, W. Watzka, U. Lange, D. Sporn, S. Gebhardt and A. Schönecker, *J. Eur. Ceram. Soc.* 2001, **21**, 1459–1462.